

MICROSCOPIC INTERFACE EFFECT ON ANTI-CROSSING BEHAVIOR and SEMICONDUCTOR-SEMIMETAL TRANSITION in InAs/GaSb SUPERLATTICES

YEN-HSIN CHAI^{a*}, KAO-FENG YARN^b, CHUN-NAN CHEN^c

^a*Department of Electrical Engineering, Technology and Science Institute of Northern Taiwan, Taipei, Taiwan, ROC*

^b*Department of Electronic Engineering, Far East University, Tainan 744, Taiwan, ROC*

^c*Department of Physics, Tamkang University, Taipei, Taiwan, ROC*

The band structures of (001), (111), and (110) InAs/GaSb superlattices in the semimetal regime are studied using a modified bond orbital model. The anti-crossing behavior between the sub-bands as well as the semiconductor-semimetal transition will be analyzed in detail, and is shown to be strongly dependent on the growth direction. The effects of interface hetero-bonds (In-Sb and Ga-As) on the InAs/GaSb superlattices are also discussed.

(Received September 16, 2009; accepted September 30, 2009)

Keywords: Semimetal, Anti-crossing, Interface effect, Bond orbital model, Superlattice, InAs/GaSb

1. Introduction

Semiconductor heterostructures made from the combination of InAs/GaSb or its variants, such as InAs/(GaIn)Sb or InAs/(AlGa)Sb, have been of considerable interest for the past decade. This is due to their broken gap type II alignment [1,2] and the application for detectors [3,4] or lasers [5,6] at tunable IR wavelengths. By varying the layer thickness, these heterostructures allow for tuning effective band gap from a semiconductor to a semimetal transition. The transition of (001)-oriented InAs/GaSb superlattices (SLs) was finely demonstrated by experiments [7-9] and predicted within theoretical models (the simplified tight-binding model, [10] the envelope function method, [11,12] and the renormalization method. [13])

Since there is no common anion or cation across the InAs/GaSb heterointerfaces, there are two possible types of interface hetero-bonds, either In-Sb or Ga-As bonds. It is currently well-established that interface heterobonds have significant effects on the electronic and optical properties of InAs/GaSb SLs. [14-17] In recent years, there are many studies and applications on the InAs/GaSb SLs or heterostructures in the semimetal regime. [18-21] Therefore, a detailed understanding of the semimetal band structures is necessary, and the influence of hetero-bonds on the semimetallic structures will be further explored.

To search a simple theoretical method for calculating the InAs/GaSb SLs, a microscopic model, the modified bond orbital model (MBOM), [22] has been proposed. This model is based on the framework of the bond orbital model (BOM) [22-25] and combines the concept of the heuristic Hbf model [14] to include the microscopic interface effect. The MBOM provides the direct insight into the microscopic symmetry of the crystal chemical bonds within the vicinity of the heterostructure interfaces, which has more physical meanings and easier manipulations in the mathematical calculations used to discuss the symmetry breaking phenomena than other methods.

Moreover, the MBOM can easily calculate various growth directions of heterostructures to explore the influence of interface perturbation which is difficult for the other methods. Thus, the MBOM is applied to study InAs/GaSb SLs grown on the (001)-, (111)-, and (110)-oriented substrates in this paper.

2. Theoretical analyses

The method used in this paper for calculating the SL band structure is based on the framework of the BOM. A detailed description of the (001)-oriented BOM had been published elsewhere. [23] To take into account the (hkl) Hamiltonian, introducing the orthogonal transformation matrix \mathbf{T} is needed, and is written as [26]

$$T = \begin{bmatrix} \cos \theta \cos \phi & \cos \theta \sin \phi & -\sin \theta \\ -\sin \phi & \cos \phi & 0 \\ \sin \theta \cos \phi & \sin \theta \sin \phi & \cos \theta \end{bmatrix} \quad (1)$$

where the angles $\theta = \tan^{-1}(\sqrt{h^2 + k^2} / l)$ and $\phi = \tan^{-1}(k / h)$ are the polar and azimuthal angles of the new growth direction relative to the primary crystallographic axes. By method of the orthogonal transformation on the wave vectors \mathbf{k} , position vectors \mathbf{R} of the unit cells, and spin-orbit coupling coefficients to the desired growth orientation, the (hkl) BOM Hamiltonian is obtained. The basic idea of the BOM is to use a layer orbital basis to express the SL Hamiltonian. Therefore, this (hkl) bulk Hamiltonian is layered to calculate the SL by the slab method. [27]

According to the Hbf concept, a microscopic model (MBOM) [22] is proposed to include the microscopic interface perturbation. The difference of the BOM and MBOM exists on the potential term: the MBOM expands the s- and p-like bond orbitals ($|\mathbf{R}, S\rangle$ and $|\mathbf{R}, \alpha\rangle$ with $\alpha = X, Y, \text{ and } Z$) in terms of the tetrahedral anti-bonding and bonding orbitals from Harrison [28] ($|\mathbf{R}, a_i\rangle$ and $|\mathbf{R}, b_i\rangle$ with $i = 1 \sim 4$), while it replaces the scalar potential with the potential operator $\hat{\mathbf{V}}$, which is expressed as

$$|\mathbf{R}, S\rangle = \sum_{i=1}^4 \frac{1}{2} |\mathbf{R}, a_i\rangle, \quad (2a)$$

$$|\mathbf{R}, \alpha\rangle = \sum_{i=1}^4 C_{\alpha}^{(i)}(\theta, \phi) |\mathbf{R}, b_i\rangle, \quad (2b)$$

and

$$\hat{\mathbf{V}} = \sum_{i=1}^4 (U^{(i)}(\mathbf{R}) |\mathbf{R}, a_i\rangle\langle\mathbf{R}, a_i| + V^{(i)}(R) |\mathbf{R}, b_i\rangle\langle\mathbf{R}, b_i|), \quad (3)$$

where $C_{\alpha}^{(i)}(\theta, \phi)$ [22] is the linear combination coefficients of $|\mathbf{R}, b_i\rangle$. $|\mathbf{R}, a_i\rangle\langle\mathbf{R}, a_i|$ and $|\mathbf{R}, b_i\rangle\langle\mathbf{R}, b_i|$ are the projection operators of the anti-bonding and bonding orbitals, and $U^{(i)}(R)$ and $V^{(i)}(R)$ are the potential energy of the conduction and valence bands for the i th chemical bond species at lattice site \mathbf{R} , respectively. Given the orthogonality [28] of the bond orbital approximation, there are

$$\langle\mathbf{R}', a_i | \mathbf{R}, a_j\rangle = \delta_{\mathbf{R}'\mathbf{R}} \delta_{ij}, \quad (4a)$$

$$\langle\mathbf{R}', a_i | \mathbf{R}, b_j\rangle = 0, \quad (4b)$$

$$\langle \mathbf{R}', b_i | \mathbf{R}, b_j \rangle = \delta_{\mathbf{R}'\mathbf{R}} \delta_{ij}. \quad (4c)$$

Inserting the expressions of Eqs. (2) and (3) into the potential term of the BOM method, the potential matrix (not a scalar potential) is obtained. This is known as the MBOM method. [22]

Through considering the three band (Γ_6^c and Γ_8^v) approximation, the SL band structure is calculated in terms of a 6×6 MBOM matrix formalism. Away from the heterojunction, all of the off-diagonal matrix elements of the potential matrix $\mathbf{V}_{6 \times 6}$ are zero, and this diagonal matrix has the same scalar potential V as typical of the BOM method. Therefore, the $\mathbf{V}_{6 \times 6}$ potential matrix is separated into the scalar potential V of host materials by adding an additional potential matrix $\Delta \mathbf{V}_{6 \times 6}$, i.e., $\mathbf{V}_{6 \times 6} = V + \Delta \mathbf{V}_{6 \times 6}$. In the low symmetry NCA heterostructures, the key difference between the MBOM and the BOM is the non-zero $\Delta \mathbf{V}_{6 \times 6}$ matrixes at the interfaces.

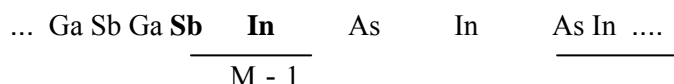
3. Results and discussion

In this section, by applying the proposed MBOM, the anti-crossing behavior and the semiconductor to semimetal transition on InAs/GaSb SLs grown on the (001)-, (111)-, and (110)-oriented substrates will be calculated and discussed. The effects of interface perturbation on InAs/GaSb SLs will be studied in detail.

3.1 For the (001) InAs/GaSb SLs

In the (u,u) (001)-oriented InAs/GaSb SLs, the planes of atoms are stacked in the growth direction as follows:

M



for the one interface; and

N - 1



N

for the next interface, where $N=M+u$. In-Sb and Ga-As hetero-bonds are found with alternatively successive existences at the interfaces. According to the MBOM, the additional potential matrixes are needed to put to the original BOM matrix at the interfaces as (in the basis ordering:

$$\omega_{1/2}, \omega_{-1/2}, \quad u_{3/2}^{3/2}, u_{1/2}^{3/2}, u_{-1/2}^{3/2}, u_{-3/2}^{3/2}$$

$$\Delta \mathbf{V}_{6 \times 6}(\mathbf{R}_Z) = \begin{bmatrix} \frac{1}{2} \Delta U & 0 & 0 & 0 & 0 & 0 \\ 0 & \frac{1}{2} \Delta U & 0 & 0 & 0 & 0 \\ 0 & 0 & \frac{1}{2} \Delta U & 0 & \frac{-i}{2\sqrt{3}} \Delta V & 0 \\ 0 & 0 & 0 & \frac{1}{2} \Delta U & 0 & \frac{-i}{2\sqrt{3}} \Delta V \\ 0 & 0 & \frac{-i}{2\sqrt{3}} \Delta V & 0 & \frac{1}{2} \Delta U & 0 \\ 0 & 0 & 0 & \frac{-i}{2\sqrt{3}} \Delta V & 0 & \frac{1}{2} \Delta U \end{bmatrix} \quad (5)$$

where R_z is the monolayer position along the growth direction, and also ΔU (for the conduction band) and ΔV (for the valence band) denote the difference of potential energy between the hetero-bond species and the host materials at the interfaces. In the MBOM model, ΔU and ΔV are the adjustable parameters. In this paper, $\Delta U = -0.36$ eV and $\Delta V = -0.56$ eV are used for the InSb/InAs junction while $\Delta U = -0.16$ eV and $\Delta V = 0.56$ eV for the GaAs/GaSb junction. [29,30] For the (27, 27) InAs/GaSb SL, the band structures along the growth direction calculated by the BOM and the MBOM are shown in Fig.1, respectively. The deviations between these two methods are mainly due to the consideration of the microscopic interface effects. [22] The three-dimensional (3D) band structures of the (40, 40) SL are performed by the BOM and MBOM, as shown in Fig.2(a) and 2(b), respectively.

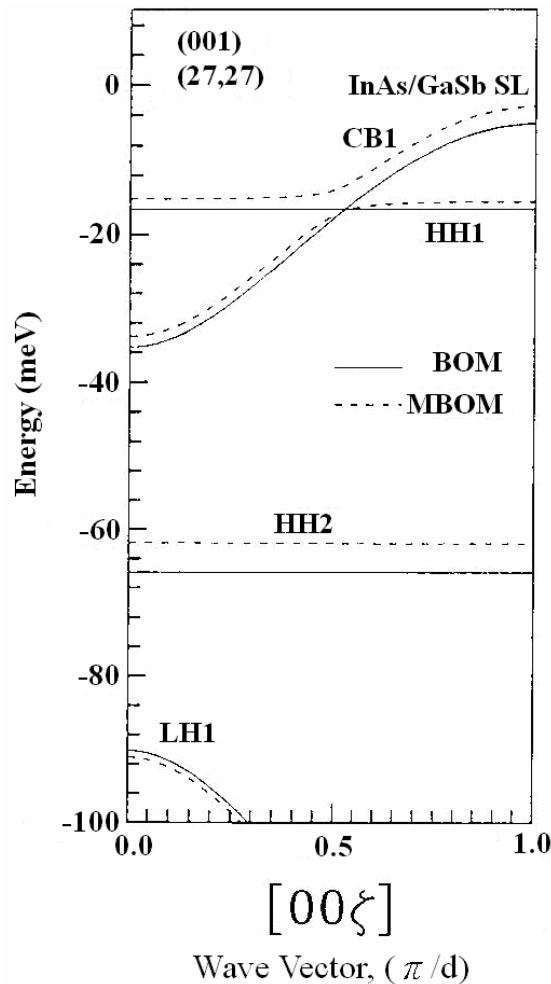
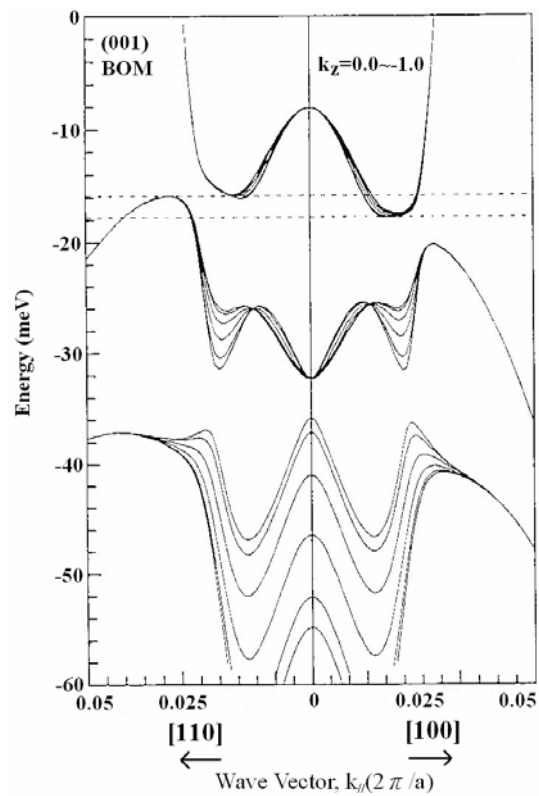
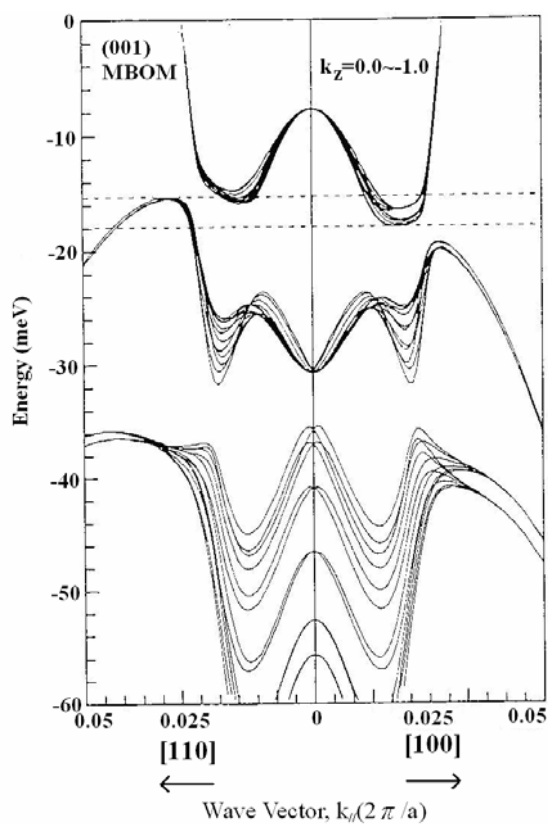


Fig. 1. Comparison of the band structures along the growth direction for the (27, 27) (001)-oriented InAs/GaSb superlattices calculated by the BOM and MBOM.



a



b

Fig. 2. The 3D band structures of the (40, 40) (001)-oriented InAs/GaSb superlattices calculated by the (a) BOM and (b) MBOM., respectively.

3.2 For the (111) InAs/GaSb SLs

For the (111)-oriented SLs, it has the same order of the atomic planes as the (001) SL. Similarly, the additional potential matrix is needed to add to the original BOM matrix at the interfaces as

$$\Delta \mathbf{V}_{6 \times 6}(\mathbf{R}_Z) = \begin{bmatrix} \frac{1}{4} \Delta U & 0 & 0 & 0 & 0 & 0 \\ 0 & \frac{1}{4} \Delta U & 0 & 0 & 0 & 0 \\ 0 & 0 & 0 & 0 & 0 & 0 \\ 0 & 0 & 0 & \frac{1}{2} \Delta V & 0 & 0 \\ 0 & 0 & 0 & 0 & \frac{1}{2} \Delta V & 0 \\ 0 & 0 & 0 & 0 & 0 & 0 \end{bmatrix} \quad (6)$$

It must be noted that Eq. (6) is at the situation of the hetero-bonds along the [111] growth direction (CASE 1). The other existing situation is that the hetero-bonds are the remaining three bonds other than the bond along the [111] direction for each interface unit cell (CASE 2). The additional potential matrixes, then, at the interfaces are shown as

$$\Delta \mathbf{V}_{6 \times 6}(\mathbf{R}_Z) = \begin{bmatrix} \frac{3}{4} \Delta U & 0 & 0 & 0 & 0 & 0 \\ 0 & \frac{3}{4} \Delta U & 0 & 0 & 0 & 0 \\ 0 & 0 & \Delta V & 0 & 0 & 0 \\ 0 & 0 & 0 & \frac{1}{2} \Delta V & 0 & 0 \\ 0 & 0 & 0 & 0 & \frac{1}{2} \Delta V & 0 \\ 0 & 0 & 0 & 0 & 0 & \Delta V \end{bmatrix} \quad (7)$$

The crossing behavior on the (21, 21) SL and the semimetal phenomenon on the (35, 35) SL are calculated by the BOM and the MBOM, as shown in Fig.3(a) and (b) and Fig.4(a)-(c), respectively.

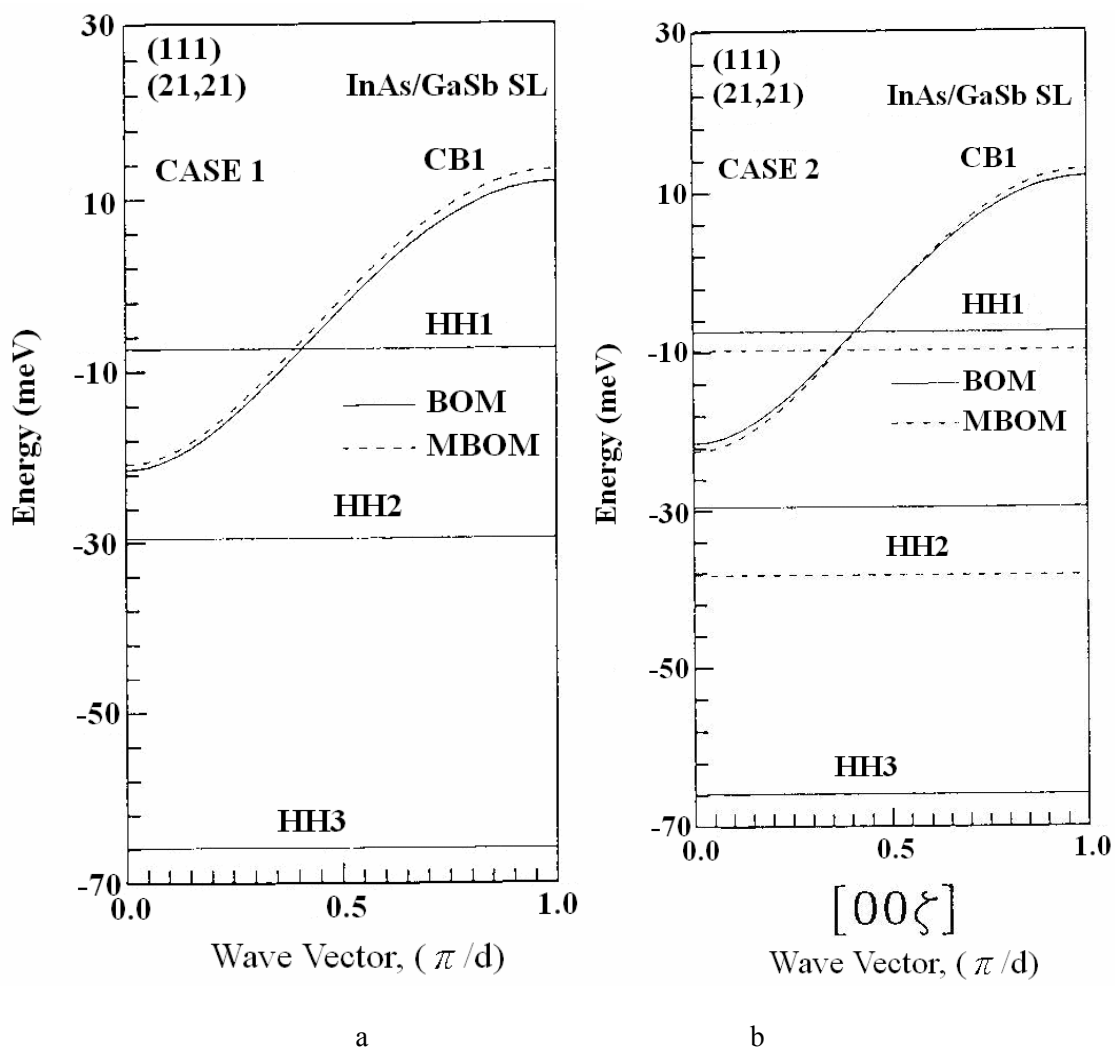


Fig. 3. The band structures along the growth direction for the $(21, 21)$ (111) -oriented InAs/GaSb superlattices calculated by the BOM and MBOM on the (a) CASE 1: at the situation of the hetero-bonds along the $[111]$ growth direction and (b) CASE 2: the remaining three hetero-bonds not the bond along the $[111]$ direction for each interface unit cell.

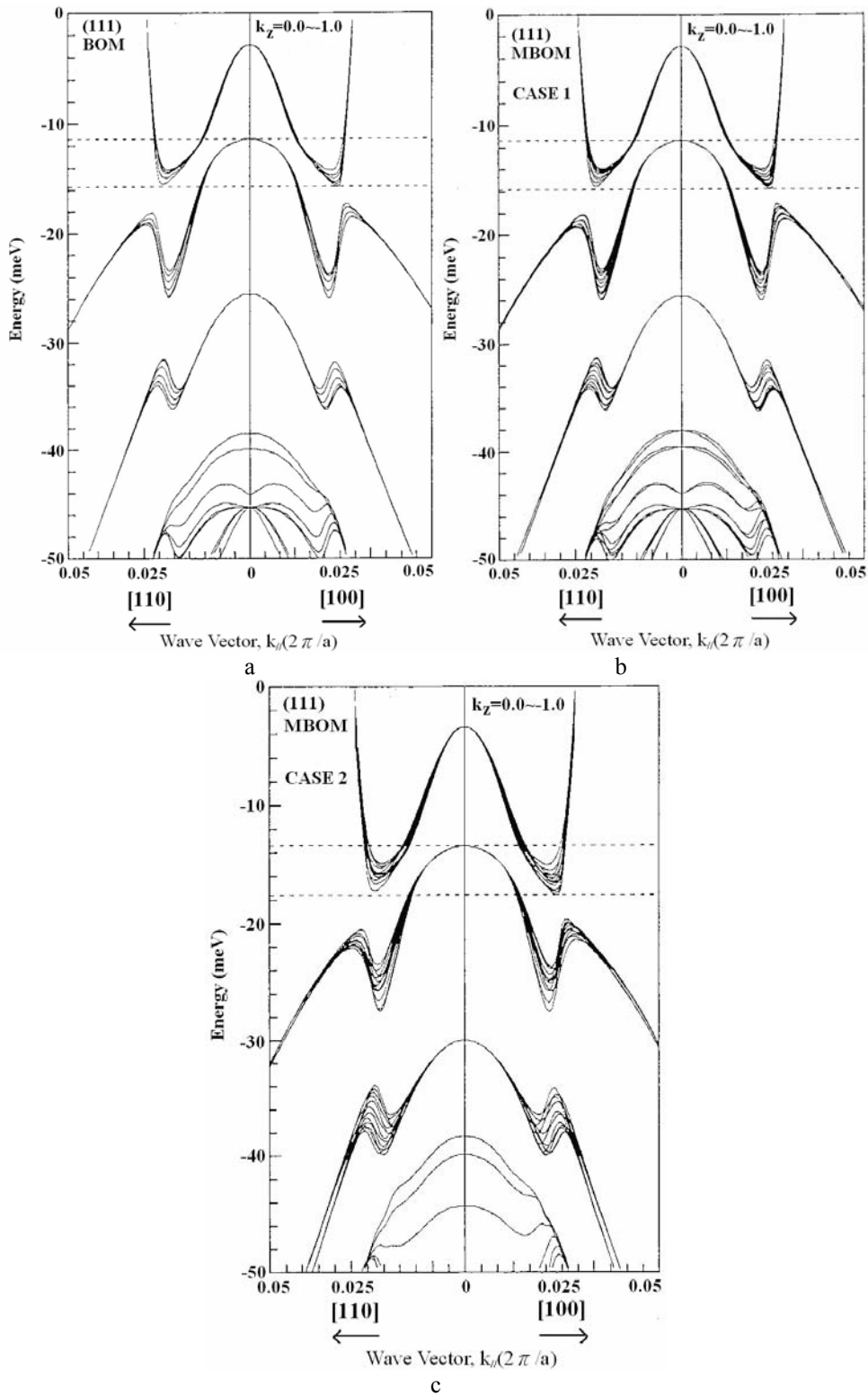
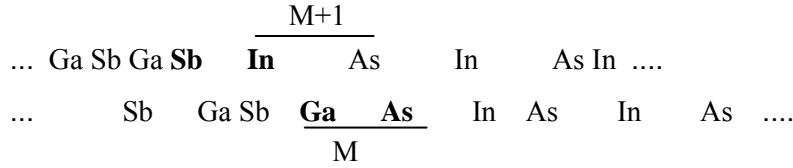


Fig. 4. The 3D band structures of the (35, 35) (111)-oriented InAs/GaSb superlattices calculated by the (a) BOM and (b) MBOM (CASE 1) and (c) MBOM (CASE 2).

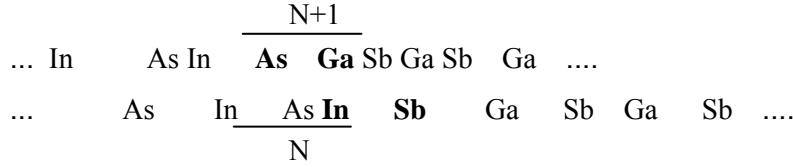
3.3 For the (110) InAs/GaSb SLs

For the (u,u) InAs/GaSb SLs grown on the (110) substrate, each interface has an equal

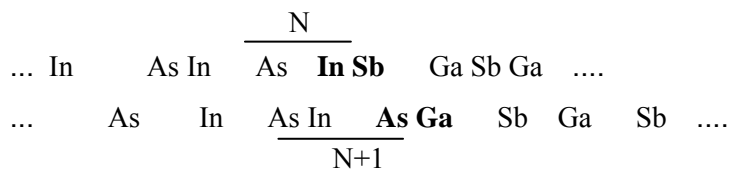
number of hetero-bonds (In-Sb and Ga-As). Across from the perfect (110) interfaces, planes of atoms are stacked along the growth direction for the one interface as:



and for the next interface as:



,if u is an even number;



,if u is an odd number. Note that the arranged atoms above are overlooked from the (001) surface. The Mth (or Nth) monolayer is located at the left (or right) interface, where $N=M+u$. Thus, the additional potential matrixes to the original BOM matrix at the interfaces are given by

$$\Delta \mathbf{V}_{6 \times 6}(\mathbf{R}_Z) = \begin{bmatrix} \frac{1}{4} \Delta U & 0 & 0 & 0 & 0 & 0 \\ 0 & \frac{1}{4} \Delta U & 0 & 0 & 0 & 0 \\ 0 & 0 & \frac{1}{8} \Delta V & \frac{\pm 1}{2\sqrt{6}} \Delta V & \frac{-1}{8\sqrt{3}} \Delta V & 0 \\ 0 & 0 & \frac{\pm 1}{2\sqrt{6}} \Delta V & \frac{3}{8} \Delta V & 0 & \frac{-1}{8\sqrt{3}} \Delta V \\ 0 & 0 & \frac{-1}{8\sqrt{3}} \Delta V & \frac{3}{8} \Delta V & \frac{\mp 1}{2\sqrt{6}} \Delta V & \frac{-1}{8\sqrt{3}} \Delta V \\ 0 & 0 & 0 & \frac{-1}{8\sqrt{3}} \Delta V & \frac{\mp 1}{2\sqrt{6}} \Delta V & \frac{1}{8} \Delta V \end{bmatrix} \quad (8)$$

Note that the upper sign of the additional matrixes is used for the Mth and Nth monolayers, and the lower sign is used for the (M+1)th and (N+1)th monolayers. For the (36, 36) InAs/GaSb SL, the anti-crossing behavior between the lowest conduction subband and the topmost valence sub-band is found, as shown in Fig.5. For the (55, 55) InAs/GaSb SL, it is in the semimetal regime, as shown in Fig.6(a) and (b).

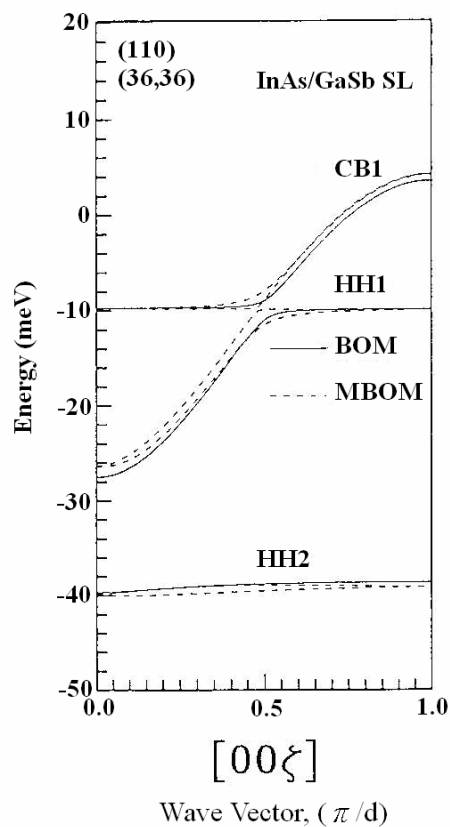


Fig. 5. The band structures along the growth direction for the (36, 36) (110)-oriented InAs/GaSb superlattices calculated by the BOM and MBOM, respectively.

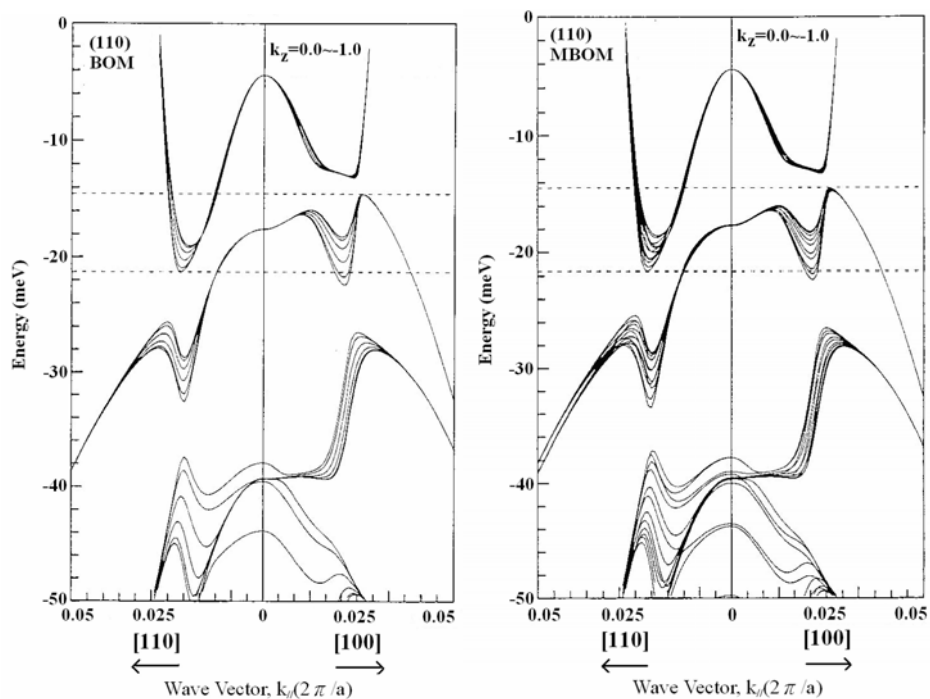


Fig. 6. The 3D band structures of the (55, 55) (110)-oriented superlattices calculated by the (a) BOM and (b) MBOM, respectively.

It is well known that along a low-symmetry direction in \mathbf{k} space, no band degeneracies are allowed, and therefore, a gap must appear between the two intersecting bands. The occurrence of crossing is only allowed along the [001] and [111] high-symmetry growth directions, and this phenomenon is confirmed by the BOM calculations. If the microscopic interface structure of InAs/GaSb SLs is considered, the MBOM results show that crossing behavior does not exist along the [001] growth direction again, but remains happening on the [111] growth direction. [31] The reason for this is the interface perturbation (hetero-bonds) results in the symmetry reduction: from D_{2d} to C_{2v} for (001) SLs and D_{3d} to C_{3v} for (111) SLs. Since the symmetry C_{2v} is not so high, the anti-crossing behavior appears along the [001] growth direction. On the contrary, the (111) SL has crossing due to remain having the high symmetry C_{3v} .

The hetero-bonds existing on the consecutive interfaces of InAs/GaSb SLs result in the interface inversion asymmetry that generates the in-plane spin splitting for arbitrary growth direction. Along the growth direction, the microscopic symmetry reduction at the interface unit-cells is due to the existence of heterobonds. The microscopic potential perturbation is found leading to the Dresselhaus-like spin splitting. The zero-field spin splitting caused by the inversion asymmetry of the microscopic crystal potential is the Dresselhaus effect: [32] the degeneracy bands of the zinc-blende bulk are lifted except for the wave vector along the $\langle 100 \rangle$ and $\langle 111 \rangle$ directions. [33] The InAs/GaSb SLs on the [001]- and [111]-growth directions still have a relatively high symmetry, even with the symmetry reduction at the interfaces,. Thus, the spin splitting exists on all the growth directions except on the (001) and (111) SLs.

The study of the 3D band structure in the semimetal regime was performed by the BOM with a microscopic description of the InAs/GaSb SLs. As the layer thicknesses increase, the lowest conduction and highest valence subbands approach each other until crossing occurs. The subband dispersion for \mathbf{k} not parallel to the axis in high-symmetry direction obeys a no-crossing rule: subbands can only cross for \mathbf{k} parallel to the SL growth axis with high symmetry. For in-plane wave vector $\mathbf{k}_{\parallel} \neq 0$, hybridization and anti-crossing behavior occurs, which open small gaps between conduction-band-like and valence-band-like subbands, i.e., the anti-crossing behavior prevents the formation of a negative gap.

For the (40, 40) (001)-oriented InAs/GaSb SL, a negative indirect gap can be obtained by the band anisotropy and the spin splitting, [13] as shown in Fig. 2(a) and (b), where the spin splitting is depicted by the MBOM, but not the BOM. For the (35, 35) (111)-oriented InAs/GaSb SL, a negative indirect gap can be observed due to the multibands coupling between the lowest conduction subband and the several higher valence subbands, as shown in Fig.4(a)-(c). Note that the negative indirect gap is nearly independent of band anisotropy, and the spin splitting is a minor role on this (111) SL. Due to the high in-plane band anisotropy, the (55, 55) (110)-oriented InAs/GaSb SL has an obvious negative indirect gap, as shown in Fig.6(a) and (b). Moreover, the indirect negative gap also occurs in the same $[\bar{1}10]$ direction, as shown in the left panel of Fig.6(b), arising from the multiband coupling by adding the spin splitting.

4. Conclusions

The crossing behavior of InAs/GaSb superlattices has been investigated. It is found that the crossing (zero gap) appears along the [001]- and [111]-growth directions. When the effects of interface perturbation are taken into account, the crossing does not occur along the [001]-growth direction again, but remain existing along the [111]-growth direction. According to the calculations, the semiconductor to semimetal transition in (001), (111), and (110) InAs/GaSb superlattices is obtained at the critical layer thickness within the vicinity of 10.5nm. The semimetal phenomenon (a negative indirect band gap) originates from three contributions: the band anisotropy, the spin splitting, and the multiband coupling. Moreover, the negative indirect band gap is found to be strongly growth-direction dependent. The results of the present paper considering the microscopic interface perturbation and the growth-direction dependent phenomena may provide the reference for future work in regards to the InAs/GaSb superlattices in the semimetal region.

Acknowledgements

The authors would like to express thanks to the Foundation of Chen Jieh-Chen Scholarship for its financial support in this work.

References

- [1] E. Halvorsen, Y. Galperin, and K. A. Chao, *Phys. Rev. B* **61**, 16743 (2000).
- [2] S. De-Leon and B. Laikhtman, *Phys. Rev. B* **61**, 2874 (2000).
- [3] H. Mohseni, E. Michel, J. Sandoen, M. Razeghi, W. Mitchel, and G. Brown, *Appl. Phys. Lett.* **71**, 1403 (1997).
- [4] D. N. Talwar, B. Jogai, and J. P. Loehr, *Mater. Sci. Eng. B* **51**, 12 (1998).
- [5] T. C. Hasenberg, R. H. Miles, A. R. Kost, and L. West, *IEEE J. Quantum Electron.* **33**, 1403 (1997).
- [6] J. R. Meyer, C. A. Hoffman, F. J. Bartoli, and L. R. Rammoban, *Appl. Phys. Lett.* **67**, 757 (1995).
- [7] L. L. Chang, *J. Phys. Soc. Jpn.* **49**, Suppl. A 997 (1980).
- [8] Y. Guldner, J. P. Vieren, P. Voisin, M. Voos, L. L. Chang, and L. Esaki, *Phys. Rev. Lett.* **45**, 1719 (1980).
- [9] S. R. White and L. J. Sham, *Phys. Rev. Lett.* **47**, 879 (1981).
- [10] G. A. Sai-Halasz, L. Esaki, and W. A. Harrison, *Phys. Rev. B* **18**, 2812 (1978).
- [11] G. Bastard, *Phys. Rev. B* **24**, 5693 (1981).
- [12] G. Bastard, *Phys. Rev. B* **25**, 7584 (1982).
- [13] G. Grosso, S. Moroni, and G. P. Parravicini, *Phys. Rev. B* **40**, 12328 (1989).
- [14] O. Krieb, and P. Voisin, *Phys. Rev. Lett.* **77**, 1829 (1996).
- [15] O. Krieb, W. Seidel, J.P. Andre, D. Bertho, C. Jouanion, and P. Voisin, *Semicond. Sci. Technol.* **12**, 938 (1997).
- [16] E. L. Ivchenko and A. A. Toropov, *Sov. Phys. Solid State* **40**, 1748 (1998).
- [17] A. V. Platonov, V. P. Kochereshko, E. L. Ivchenko, and G. V. Hikhailov, *Phys. Rev. Lett.* **83**, 3546 (1999).
- [18] A. J. L. Poulter, M. Lakrimi, R. J. Nicholas, N. J. Mason, and P. J. Walker, *Phys. Rev. B* **59**, 10785 (1999).
- [19] S. A. Emel'yanov, Y. A. Terent'ev, A. P. Dmitriev, and B. Y. Meptser, *JETP Lett.* **68**, 810 (1998).
- [20] R. J. Wagner, B. V. Shanabrook, M. J. Yang, and J. R. Waterman, *Superlatt. Microstruct.* **21**, 95 (1997).
- [21] K. D. Moiseev, M. P. Mikhailova, N. D. Stoyanov, Y. P. Yakovlev, E. Hulicius, T. Simecek, J. Oswald, and J. Pangrac, *J. Appl. Phys.* **86**, 6264 (1999).
- [22] C. N. Chen, Y. H. Wang, M. P. Houg, and J. C. Chiang, *Jpn. J. Appl. Phys. Part 1* **41**, 36 (2002).
- [23] Y. C. Chang, *Phys. Rev. B* **37**, 8215 (1988).
- [24] M. P. Houg and Y. C. Chang, *J. Appl. Phys.* **64**, 4609 (1988).
- [25] J. S. Shyu and J. C. Chiang, *Phys. Rev. B* **60**, 1799 (1999).
- [26] A. Niwa, T. Ohtoshi, and T. Kuroda, *IEEE J. Selected Topics Quantum Electron.* **1**, 211 (1995).
- [27] J. N. Schulman and T. C. McGill, *Phys. Rev. Lett.* **39**, 1680 (1977).
- [28] W. A. Harrison, *Electronic structure and the Properties of Solids*, (Dover, New York, 1989).
- [29] J. R. Waterman, B. V. Shanabrook, R. J. Wagner, M. J. Yang, J. L. Davis, and J. P. Omaggio, *Semicond. Sci. Technol.* **8**, S106 (1993).
- [30] G. Edwards, J. C. Inkson, *Semicond. Sci. Technol.* **9**, 178 (1994).
- [31] D. L. Smith, C. Mailhiot, *J. Appl. Phys.* **62**, 2545 (1987).
- [32] G. Dresselhaus, *Phys. Rev.* **100**, 580 (1955).
- [33] R. Eppenga, M. F. H. Schuurmans, *Phys. Rev. B* **37**, 10923 (1988).